

Journal Pre-proofs

Full Length Article

Analytical method of nonlinear coupled constitutive relations for rarefied non-equilibrium flows

Zhiqiang He, Zhongzheng Jiang, Huangwei Zhang, Weifang Chen

PII: S1000-9361(20)30312-5
DOI: <https://doi.org/10.1016/j.cja.2020.06.023>
Reference: CJA 1672

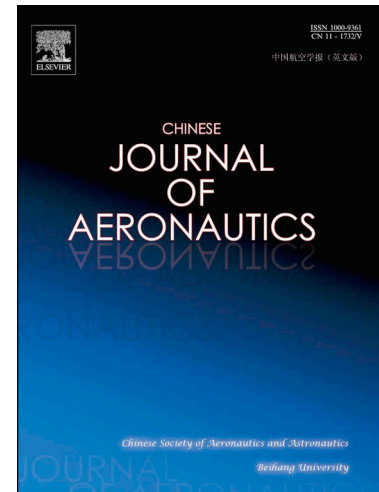
To appear in: *Chinese Journal of Aeronautics*

Received Date: 15 January 2020
Revised Date: 23 June 2020
Accepted Date: 23 June 2020

Please cite this article as: Z. He, Z. Jiang, H. Zhang, W. Chen, Analytical method of nonlinear coupled constitutive relations for rarefied non-equilibrium flows, *Chinese Journal of Aeronautics* (2020), doi: <https://doi.org/10.1016/j.cja.2020.06.023>

This is a PDF file of an article that has undergone enhancements after acceptance, such as the addition of a cover page and metadata, and formatting for readability, but it is not yet the definitive version of record. This version will undergo additional copyediting, typesetting and review before it is published in its final form, but we are providing this version to give early visibility of the article. Please note that, during the production process, errors may be discovered which could affect the content, and all legal disclaimers that apply to the journal pertain.

© 2020 Production and hosting by Elsevier Ltd. on behalf of Chinese Society of Aeronautics and Astronautics.



Contents lists available at [ScienceDirect](https://www.sciencedirect.com)

Chinese Journal of Aeronautics

journal homepage: www.elsevier.com/locate/cja

Analytical method of nonlinear coupled constitutive relations for rarefied non-equilibrium flows

Zhiqiang HE ^{a,b}, Zhongzheng JIANG ^a, Huangwei ZHANG ^b, Weifang CHEN ^{a,*}

^a School of Aeronautics and Astronautics, Zhejiang University, Hangzhou 310027, China

^b Department of Mechanical Engineering, National University of Singapore, Singapore 117576, Singapore

Received 17 January 2020; revised 21 April 2020; accepted 10 May 2020

Abstract

It is well known that Navier-Stokes equations are not valid for those high-Knudsen and high-Mach flows, in which the local thermodynamically non-equilibrium effects are dominant. To extend the non-equilibrium describing the ability of macroscopic equations, Nonlinear Coupled Constitutive Relation (NCCR) model was developed from Eu's generalized hydrodynamic equations to substitute linear Newton's law of viscosity and Fourier's law of heat conduction in conservation laws. In the NCCR model, how to solve the decomposed constitutive equations with reasonable computational cost is a key ingredient of this scheme. In this paper, an analytic method is proposed firstly. Compared to the iterative procedure in the conventional NCCR model, the analytic method not only obtains exact roots of the decomposed constitutive polynomials, but also preserves the nonlinear constitutive relations in the original framework of NCCR methods. Numerical tests to assess the efficiency and accuracy of the proposed method are conducted for argon shock structures, Couette flows, two-dimensional hypersonic flows over a cylinder and three-dimensional supersonic flows over a three-dimensional sphere. These superior advantages of the current method are expected to render itself a powerful tool for simulating the hypersonic rarefied flows and microscale flows of high Knudsen number for engineering applications.

Keywords: Nonlinear constitutive relations; Non-equilibrium; Rarefied gas; Microscale flow; Knudsen number

^{a*}Corresponding author.

E-mail address: chenwfhudt@163.com

1. Introduction

A deep reform has been taking place in the field of fluid mechanics in the past half century, during which the scope of fluid mechanics is extended from macro to micro and also from the ground to the space. As the altitude increases, the air density decreases gradually and the mean free path of the air molecules can be comparable to the relevant characteristic length scale of the studied problems. The Knudsen number (Kn), defined as the ratio of molecule mean free path to characteristic length, can be used to divide four

different flow regimes, i.e. continuum regime, slip regime, transition regime and free molecular flow regime, corresponding to $Kn \leq 0.01$, $0.01 < Kn \leq 0.1$, $0.1 < Kn \leq 10$, and $Kn > 10$, respectively¹. In continuum regime and slip regime, Navier-Stokes (N-S) equations are always employed on the wall with slip boundary conditions to account for the local rarefied effect. However, as the mean free path continuously increases, N-S equations would be not valid in the transition and free molecular flow regimes. It indicates that the linear constitutive relations in conjunction with the slip boundary condition are not sufficient to capture the nonlinear velocity distribution within the Knudsen layer

and the multi-scale flows²⁻⁴ away from wall such as the strong shock wave structure^{5, 6}, microscale flow, flow separation and wake flows.

Boltzmann equation is the core of study in the rarefied nonequilibrium flow. It describes the statistical behaviour of a thermodynamic system deviating from equilibrium state and thus can describe all of the four flow regimes mentioned above. However, there are many challenges in solving the Boltzmann equation because of its complex collision term. To accurately simulate the non-equilibrium dynamics, many effective theories and numerical methods are proposed based on Boltzmann equation. One of them is stochastic particle methods, such as Direct Simulation Monte Carlo (DSMC)^{7, 8} method which has always been used as a standard for validating other methods in numerical simulations. DSMC is recognized as the most reliable method for flows of high Knudsen number. However, DSMC faces stochastic fluctuation in low-speed flows and prohibitively high computational costs in the near-continuum regime due to the limitation of time steps and cell sizes. The others include deterministic method, such as Discrete Velocity Method (DVM)^{9, 10}, Fast Spectral Method (FSM)¹¹, Unified Gas-Kinetic Scheme (UGKS)¹²⁻¹⁴, Discrete Unified Gas Kinetic Scheme (DUGKS)^{15, 16} and Gas-Kinetic Unified Algorithm (GKUA)¹⁷⁻¹⁹. There is no stochastic fluctuation issue in these methods, but heavy computational cost caused by velocity space discretization inhibits its wide engineering application, especially for hypersonic flows.

Chapman-Enskog expansion method²⁰⁻²² and moment method²³⁻²⁷ extend the scope of N-S equations from the continuum regime to those flows which are not far from the equilibrium. Burnett equations and Grad-type equations are the most representative ones of them^{25, 28, 29}. However, Grad's 13-moment equations encounter non-physical sub-shock problems beyond a critical Mach number^{30, 31} and conventional Burnett equations are contradictory to Gibbs relation^{32, 33} in some terms. They also violate the second law of thermodynamics, and encounter computational instability under some unfavorable conditions. These unsatisfactory properties limit their prediction ability in high-speed and low-density flow regimes. Some measures were also taken to remedy these methodologies, for example, the Simplified Conventional Burnett (SCB) for multidimensional hypersonic flow²², the regularized 13-moment equations²³ (R13) and regularized 26 moment equations³⁴ (R26). However, many problems still exist, e.g. complex additional higher boundary conditions.

To minimize the deficiency of the N-S equations in the rarefied regime and overcome the instability and efficiency problems of other methods, Eu proposed Generalized Hydrodynamic Equations (GHEs)³⁵⁻³⁸. In Eu's theory, the kinetic theory is strictly connected to

extended irreversible thermodynamics. Through constructing a non-equilibrium canonical distribution function to connect entropy production with dissipative evolution of macroscopic non-conserved variables, the GHE is strictly enforced to be consistent with the second law of thermodynamics, which includes a set of evolution equations based on the distribution function within the framework of 13 moments. GHE has been successfully applied to calculate the shock structure profile for high Mach numbers and it gave results in good agreement with experiments³⁹. A linearized version of GHE was also used to study sound wave absorption and dispersion in molecular gases⁴⁰, which yielded good agreement with experimental data in nitrogen, hydrogen, deuterium, and HD (hydrogen-deuterium). However, it is very difficult to extend GHE to multi-dimensional problems because of the existence of the highly nonlinear coupled complicated terms for non-conserved variables, which limits its application in modern computational fluid dynamics.

To solve multidimensional problems efficiently, Eu and Myong simplified GHE to a nonlinear algebraic system using adiabatic assumption³⁹ and balance closure⁴¹, which is called as Nonlinear Coupled Constitutive Relations (NCCRs). By decoupling NCCR into two directions, i.e. the compression expansion direction and the shear direction, the decomposed algebraic system can be solved by the iterative method⁴². One-dimensional shock wave structure and two-dimensional flat plate flow problems for monatomic gases have been used to validate the capability of the NCCR model in capturing the flow physics of high-speed and low-density flow regions⁴³.

Subsequently, the NCCR model was extended to a diatomic gas by considering excess normal stress associated with the bulk viscosity of gas and was adopted successfully in the two-dimensional hypersonic rarefied flow around a blunt body⁴⁴. More investigations⁴⁵⁻⁵¹ have been performed, including a discontinuous Galerkin method on unstructured grid developed for NCCR model⁴⁹⁻⁵¹, an undecomposed NCCR solver developed by Jiang et al. in three-dimensional implicit Finite-Volume Method (FVM) framework⁵²⁻⁵⁶ and a new enhanced wall boundary condition based on NCCR model for micro-Couette flow⁵⁷. Even though NCCR model is considerably simplified compared to original GHE, it is still difficult to be implemented and solved. One has to use iterative method to solve NCCR because of its high nonlinearity, which leads to the twice to three times higher computational cost compared to that of N-S equations.

In the present work, to overcome the foregoing complexity and inefficiency of the NCCR iterative solver, we aim to develop a simplified analytical method for the NCCR model. It is realized by

expanding the nonlinear factor of the NCCR model around the equilibrium state and retaining the relevant terms until the second order of accuracy. After the simplification, the traditional nonlinear coupled constitutive relations can be solved by analytical method instead of the iterative one. Therefore, the new method is more efficient and also preserves the capability of describing non-equilibrium flows. The rest of the paper is structured as below. Nonlinear coupled constitutive relations and conventional iterative method are introduced in Section 2. The expansion and truncation of the nonlinear factor are then presented in Section 3 to obtain the analytical method and comparison with the iterative method. In Section 4, benchmark test cases are conducted to assess the accuracy and efficiency of the proposed model, which are followed by the conclusions in Section 5.

2. Governing equation

2.1. Generalized hydrodynamic equations and nonlinear coupled constitutive relations

The governing equations of conserved variables (i.e. ρ , $\rho\mathbf{u}$ and ρE in Eq.(1)) and non-conserved variables (i.e. $\mathbf{\Pi}$ and \mathbf{Q} in Eqs. (2) and (3)) for monatomic gases, i.e. Eu's generalized hydrodynamic equations³⁶, read

$$\begin{cases} \frac{\partial \rho}{\partial t} + \nabla \cdot (\rho \mathbf{u}) = 0 \\ \frac{\partial \rho \mathbf{u}}{\partial t} + \nabla \cdot (\rho \mathbf{u} \mathbf{u} + p \mathbf{I}) + \nabla \cdot \mathbf{\Pi} = 0 \\ \frac{\partial \rho E}{\partial t} + \nabla \cdot [(\rho E + p) \mathbf{u}] + \nabla \cdot (\mathbf{\Pi} \cdot \mathbf{u} + \mathbf{Q}) = 0 \end{cases} \quad (1)$$

$$\rho \frac{D(\mathbf{\Pi} / \rho)}{Dt} + \nabla \cdot \psi_2 = -2[\mathbf{\Pi} \cdot \nabla \mathbf{u}]^{(2)} - \frac{p}{\eta} \mathbf{\Pi} q(\kappa) + 2p[\nabla \mathbf{u}]^{(2)} \quad (2)$$

$$\begin{aligned} \rho \frac{D(\mathbf{Q} / \rho)}{Dt} + \nabla \cdot \psi_3 = & -\mathbf{\Pi} \cdot c_p \nabla T - \mathbf{Q} \cdot \nabla \mathbf{u} - pc_p T \nabla \ln T \\ & + \nabla \cdot (p \mathbf{I} + \mathbf{\Pi}) \cdot \frac{\mathbf{\Pi}}{\rho} - \frac{pc_p}{\lambda} \mathbf{Q} q(\kappa) \end{aligned} \quad (3)$$

Here t is time, $\nabla(\cdot)$ is the divergence and $D(\cdot)/Dt$ is the material derivative. ρ is the density, \mathbf{u} is the velocity vector of the fluid, p is the pressure, T is the temperature, \mathbf{I} is the unit tensor, E is the total energy per unit mass, $\mathbf{\Pi}$ is the shear stress tensor, \mathbf{Q} is the heat flux vector, c_p is the specific heat capacity, λ is the thermal conductivity, η is the

dynamic viscosity, and ψ_2 and ψ_3 are the higher-order moments^{36, 42}. $q(\kappa)$ in Eq. (3) is the nonlinear factor related to entropy production^{38, 42}, which takes the following form:

$$q(\kappa) = \frac{\sinh(\kappa)}{\kappa} \quad (4)$$

where κ can be specified as a Rayleigh dissipation function³⁶

$$\kappa = \frac{(mk_B)^{1/4}}{\sqrt{2}d} \cdot \frac{T^{1/4}}{p} \left(\frac{\mathbf{\Pi} : \mathbf{\Pi}}{2\eta} + \frac{\mathbf{Q} \mathbf{Q}}{\lambda} \right)^{1/2} \quad (5)$$

Here κ is related to the degree of nonequilibrium⁴⁷, m is the mass of a molecule, k_B denotes the Boltzmann constant, and d is the mean diameter of the molecule. Also, in Eq. (5), “:” means the double inner product of two second-order tensors.

Based on Eu's closure⁴⁰ and Myong's balanced closure⁴¹, the unclosed high-order terms $\nabla \psi_2$ and $\nabla \psi_3$ in Eqs. (2) and (3) are assumed to be zero. Moreover, since the non-conserved variables evolve faster than the conserved variables⁴⁰, the steady-state assumption can be introduced for the equations of the non-conserved variables, i.e. Eqs. (2) and (3). Meanwhile, the conserved variables can be assumed to be constant within the time scale of change of non-conserved variables. This is adiabatic approximation⁴⁰. Hence, we can neglect the material derivative terms, i.e. the first terms on the left-hand side of Eqs. (2) and (3). Following Myong's work^{43, 44}, the terms $\mathbf{Q} \nabla \mathbf{u}$ and $\nabla(p \mathbf{I} + \mathbf{\Pi}) \mathbf{\Pi} / \rho$ can also be neglected in Eq.(3) for simplicity. In fact, it has been confirmed that these two terms have relatively small influence on predictions of the one-dimensional shock wave structures⁵⁸. Therefore, based on the assumptions mentioned above, the algebraic equations of the non-conserved variables $\mathbf{\Pi}$ and \mathbf{Q} , i.e. NCCR model, can be derived for monatomic gas from Eqs. (2) and (3) as

$$\begin{cases} -2[\mathbf{\Pi} \cdot \nabla \mathbf{u}]^{(2)} - \frac{p}{\eta} \mathbf{\Pi} q(\kappa) - 2p[\nabla \mathbf{u}]^{(2)} = 0 \\ -\mathbf{\Pi} c_p \nabla T - \frac{pc_p}{\lambda} \mathbf{Q} q(\kappa) - pc_p T \nabla \ln T = 0 \end{cases} \quad (6)$$

The following dimensionless variables and parameters are introduced:

$$\left\{ \begin{array}{l} x^* = \frac{x}{L_0}, y^* = \frac{y}{L_0}, z^* = \frac{z}{L_0}, u^* = \frac{u}{a_\infty}, v^* = \frac{v}{a_\infty} \\ w^* = \frac{w}{a_\infty}, p^* = \frac{p}{\rho_\infty a_\infty^2}, \rho^* = \frac{\rho}{\rho_\infty}, T^* = \frac{T}{T_\infty}, \eta^* = \frac{\eta}{\eta_\infty} \\ \lambda^* = \frac{\lambda}{\lambda_\infty}, E^* = \frac{E}{a_\infty^2}, h^* = \frac{h}{a_\infty^2}, t^* = \frac{t}{L_0 / a_\infty} \\ R^* = \frac{R}{a_\infty^2 / T_\infty} = \frac{1}{\gamma}, c_p^* = \frac{c_p}{a_\infty^2 / T_\infty} = \frac{1}{\gamma - 1} \\ \Pi^* = \frac{\Pi}{\eta_\infty a_\infty / L_0}, \mathcal{Q}^* = \frac{\mathcal{Q}}{\lambda_\infty T_\infty / L_0} \end{array} \right. \quad (7)$$

where L_0 is the reference length, a is the speed of sound, h is the total enthalpy per unit mass, R is the specific gas constant, and γ is the specific heat ratio. Here quantities with subscripts “ ∞ ” represent the inflow parameters, whilst the superscript of the asterisks denotes the dimensionless parameters, which will be omitted below for brevity.

With Eq. (7), the dimensionless governing equations of the conserved variables, i.e. Eq. (1), for monatomic gas read

$$\frac{\partial \mathbf{U}}{\partial t} + \nabla \mathbf{F}_c + N_\delta \nabla \cdot \mathbf{v} = 0$$

$$\mathbf{U} = \begin{bmatrix} \rho \\ \rho \mathbf{u} \\ \rho E \end{bmatrix}, \mathbf{F}_c = \begin{bmatrix} \rho \mathbf{u} \\ \rho \mathbf{u} \mathbf{u} + p \mathbf{I} \\ (\rho E + p) \mathbf{u} \end{bmatrix}, \mathbf{F}_v = \begin{bmatrix} 0 \\ \Pi \\ \Pi \mathbf{u} + \varepsilon \mathcal{Q} \end{bmatrix} \quad (8)$$

where \mathbf{U} is the solution vector of conserved variables, \mathbf{F}_c is the inviscid flux vector, and \mathbf{F}_v is the flux vector related to the non-conserved variables. N_δ and ε are given by

$$\left\{ \begin{array}{l} N_\delta = \frac{Ma}{Re} \\ \varepsilon = \frac{1}{Pr(\gamma - 1)} \end{array} \right. \quad (9)$$

The Prandtl number Pr in Eq. (9) is assumed to be constant, and for monatomic gases, $Pr = 2/3$. The Mach number (Ma) and Reynolds number (Re) are defined as

$$Ma = \frac{u_\infty}{a_\infty}, Re = \frac{\rho_\infty u_\infty L_0}{\eta_\infty} \quad (10)$$

With Eq. (7), the NCCR model, i.e. Eq. (6), can be recast into the following non-dimensional form:

$$\hat{\Pi} q(c\hat{R}) = \hat{\Pi}_0 + [\hat{\Pi} \nabla \hat{\mathbf{u}}]^{(2)}, \hat{\mathcal{Q}} q(c\hat{R}) = \hat{\mathcal{Q}}_0 + \hat{\Pi} \hat{\mathcal{Q}} \quad (11)$$

Here c is a variable determined by the type of gas molecules⁴²; for a rigid elastic spherical molecule, $c = 1.1908$; for argon, $c = 1.0179$; for a Maxwellian molecule, $c = 1.0138$. $q(\kappa)$ in Eq. (4) is recast into

$q(c\hat{R})$. The quantities with carets in Eq. (11) are

$$\left\{ \begin{array}{l} \hat{\Pi} = \frac{N_\delta}{p} \Pi \\ \hat{\mathcal{Q}} = \frac{N_\delta}{p} \frac{\mathcal{Q}}{\sqrt{T/(2\varepsilon)}} \\ \hat{R} = (\hat{\Pi} : \hat{\Pi} + \hat{\mathcal{Q}} \hat{\mathcal{Q}})^{1/2} \\ \nabla \hat{\mathbf{u}} = -2\eta \frac{N_\delta}{p} \nabla \mathbf{u} \end{array} \right. \quad (12)$$

Moreover, $\hat{\Pi}_0$ and $\hat{\mathcal{Q}}_0$ in Eq.(11) respectively represent the trace-free shear stress from linear Newtonian law and the heat conduction from linear Fourier's law, whose original forms without caret are

$$\Pi_0 = -2\eta \mathbf{u}^{(2)}, \mathcal{Q}_0 = -\lambda \nabla T \quad (13)$$

2.2. Decomposed algebraic system for NCCR model

The dimensionless NCCR model, i.e. Eq. (11), is a set of algebraic equations with high nonlinearity and is difficult to be solved, even though it has been greatly simplified from GHE³⁶. A decomposed nonlinear algebraic system of the NCCR model was proposed by Myong⁴², which can be solved by an iterative method. The iterative process of the NCCR model does not need to solve a coupled hyperbolic system with higher-order variables such as Grad's 13-moment equations²⁵, but only requires an additional procedure to calculate the stress and heat flux from the decomposed nonlinear algebraic system separately and then implement them in the equations of the conserved variables, i.e. Eq. (8), which shares a similar feature with the traditional N-S equation to solve the five components of conserved moments. Although Jiang et al. developed an undecomposed hybrid algorithm for NCCR⁵⁴, its intrinsic complexity renders it difficult to be implemented. Also, its convergence characteristic has not been tested and therefore is still not clear. Nevertheless, Myong's decomposed solver can be mathematically proved to be converged and seems easy for implementation. Therefore, the decomposed solver by Myong⁴² will be adopted in the current work.

Based on Myong's decomposed algorithm⁴², three-dimensional problem can be decoupled approximately into three one-dimensional problems in x , y and z directions, i.e., $(\hat{\Pi}_{xx}, \hat{\Pi}_{yy}, \hat{\Pi}_{zz}, \hat{\Pi}_{xy}, \hat{\Pi}_{yz}, \hat{\mathcal{Q}}_x, \hat{\mathcal{Q}}_y, \hat{\mathcal{Q}}_z)$ is decomposed into, $(\hat{\Pi}_{xx}, \hat{\Pi}_{xy}, \hat{\Pi}_{xz})$, $(\hat{\Pi}_{xy}, \hat{\Pi}_{yy}, \hat{\Pi}_{yz}, \hat{\mathcal{Q}}_y)$ and $(\hat{\Pi}_{xz}, \hat{\Pi}_{yz}, \hat{\Pi}_{zz}, \hat{\mathcal{Q}}_z)$. In x direction, the shear stress and heat flux components $(\hat{\Pi}_{xx}, \hat{\Pi}_{xy}, \hat{\Pi}_{xz}, \hat{\mathcal{Q}}_x)$ on a surface in three-dimensional

finite volume method induced by thermodynamic forces (u_x, v_x, w_x, T_x) can be approximated as the sum of two decomposed solvers: one on $(u_x, 0, 0, T_x)$ describing the compression and expansion flows, and the other on

$(0, v_x, 0, 0)$ and $(0, 0, w_x, 0)$ describing shear flows. In order to give a brief decomposed solution process for three-dimensional monatomic NCCR model, we take a unified notation here⁵⁴ and a rotation index is introduced firstly in Table 1.

Table 1 Description of unified notation and rotation index.

i	x_i	u_i	j	x_j	u_j	k	x_k	u_k
1	x	u	2	y	v	3	z	w
2	y	v	3	z	w	1	x	u
3	z	w	1	x	u	2	y	v

2.2.1. Compression and expansion solver

The decomposed solver in the normal direction i of x_i plane is given by

$$\begin{aligned} q(c\hat{R})\hat{I}_{x_i x_i}^{u_{i,j}} &= (1 + \hat{I}_{x_i x_i}^{u_{i,i}})\hat{I}_{x_i x_i, 0}^{u_{i,j}} \\ q(c\hat{R})\hat{Q}_{x_i} &= (1 + \hat{I}_{x_i x_i}^{u_{i,i}})\hat{Q}_{x_i, 0} \end{aligned} \quad (14)$$

where

$$\hat{R}^2 = \frac{3}{2}(\hat{I}_{x_i x_i}^{u_{i,i}})^2 + \hat{Q}_{x_i}^2 \quad (15)$$

Variables with the subscript 0 correspond to stress from linear Newtonian law and the heat conduction from linear Fourier's law.

2.2.2. Shear flow solver

The decomposed solver in the two shear directions j and k of x_i plane is

$$\begin{cases} q(c\hat{R}_{ij})\hat{I}_{x_i x_j}^{u_{j,i}} = -\frac{2}{3}\hat{I}_{x_i x_j}^{u_{j,i}}\hat{I}_{x_i x_j, 0}^{u_{j,i}} \\ q(c\hat{R}_{ij})\hat{I}_{x_i x_j}^{u_{j,i}} = (1 + \hat{I}_{x_i x_j}^{u_{j,i}})\hat{I}_{x_i x_j, 0}^{u_{j,i}} \end{cases} \quad (16)$$

And

$$\begin{cases} q(c\hat{R}_{ik})\hat{I}_{x_i x_k}^{u_{k,i}} = -\frac{2}{3}\hat{I}_{x_i x_k}^{u_{k,i}}\hat{I}_{x_i x_k, 0}^{u_{k,i}} \\ q(c\hat{R}_{ik})\hat{I}_{x_i x_k}^{u_{k,i}} = (1 + \hat{I}_{x_i x_k}^{u_{k,i}})\hat{I}_{x_i x_k, 0}^{u_{k,i}} \end{cases} \quad (17)$$

where

$$\begin{cases} \hat{R}_{ij}^2 = 3\hat{I}_{x_i x_j}^{u_{j,i}}(\hat{I}_{x_i x_j}^{u_{j,i}} - 1) \\ \hat{R}_{ik}^2 = 3\hat{I}_{x_i x_k}^{u_{k,i}}(\hat{I}_{x_i x_k}^{u_{k,i}} - 1) \end{cases} \quad (18)$$

2.2.3 Recombination of two decomposed solvers

The two decomposed solvers can be solved with the iterative method proposed by Myong and more details

can be found in Refs.^{42, 54} After obtaining the iterative solutions in three dimensions, all non-conserved variables (e.g. $\hat{I}_{xx}^{u_x}$ and \hat{Q}_x) are summed at the current time step as

$$\begin{aligned} \Pi_{xx} &= \frac{p}{N_\delta} \left[\begin{aligned} &\hat{I}_{xx}^{u_x} + \hat{I}_{xx}^{v_x} + \hat{I}_{xx}^{w_x} - \frac{\hat{I}_{yy}^{v_y} + \hat{I}_{zz}^{w_z}}{2} \\ &-2(\hat{I}_{yy}^{u_y} + \hat{I}_{zz}^{u_z}) + \hat{I}_{yy}^{w_y} + \hat{I}_{zz}^{v_z} \end{aligned} \right] \\ \Pi_{yy} &= \frac{p}{N_\delta} \left[\begin{aligned} &\hat{I}_{yy}^{v_y} + \hat{I}_{yy}^{u_y} + \hat{I}_{yy}^{w_y} - \frac{\hat{I}_{xx}^{u_x} + \hat{I}_{zz}^{w_z}}{2} \\ &-2(\hat{I}_{xx}^{v_x} + \hat{I}_{zz}^{v_z}) + \hat{I}_{xx}^{w_x} + \hat{I}_{zz}^{u_z} \end{aligned} \right] \end{aligned} \quad (19)$$

$$\Pi_{zz} = -(\Pi_{xx} + \Pi_{yy})$$

$$\Pi_{xy} = \Pi_{yx} = \frac{p}{N_\delta}(\hat{I}_{xy}^{v_x} + \hat{I}_{yx}^{u_y})$$

$$\Pi_{xz} = \Pi_{zx} = \frac{p}{N_\delta}(\hat{I}_{xz}^{w_x} + \hat{I}_{zx}^{u_z})$$

$$\Pi_{yz} = \Pi_{zy} = \frac{p}{N_\delta}(\hat{I}_{yz}^{w_y} + \hat{I}_{zy}^{v_z})$$

$$Q_x = \frac{p\sqrt{T/(2\varepsilon)}}{N_\delta}\hat{Q}_x$$

$$Q_y = \frac{p\sqrt{T/(2\varepsilon)}}{N_\delta}\hat{Q}_y \quad (20)$$

$$Q_z = \frac{p\sqrt{T/(2\varepsilon)}}{N_\delta}\hat{Q}_z$$

Then substitute these variables back into the conserved variable equation, i.e. Eq. (8), to continue the time marching.

3. Analytical NCCR model

Although the NCCR model has been simplified and decomposed compared to the Eu's original equations⁴², its numerical solution is still not straightforward to be obtained due to its high nonlinearity. Conventional iterative algorithms include the fixed-point iterative method, Newton's method, and coupled method⁵⁴.

However, all these methods need numerous iteration steps to obtain the converged solutions from the initial conditions and may diverge under some unfavorable conditions.

To overcome the deficiency of the iterative method, we will develop an analytical method for the NCCR model in this work. Since c is a positive value close to 1 and \hat{R} can be used to measure the degree of nonequilibrium⁴⁷, we start with the Taylor expansion at $c\hat{R} = 0$ for the nonlinear factor $q(c\hat{R})$ in Eqs. (2) and (3), i.e.,

$$q(c\hat{R}) = \frac{\sinh(c\hat{R})}{c\hat{R}} = 1 + \frac{(c\hat{R})^2}{6} + \mathcal{O}[(c\hat{R})^3] \quad (21)$$

where \sinh is hyperbolic sine function and $\mathcal{O}[(c\hat{R})^3]$ means a higher order infinitesimal of $(c\hat{R})^3$.

For flows in near space or in micro-electro-mechanical systems where the rarefaction and non-equilibrium effects are not as strong as those in highly transitional flows and free molecular flows¹, the higher-order terms at the left-hand side of Eq. (21) can be truncated, and only the first- and second-order terms are retained, i.e.

$$q(c\hat{R}) \approx 1 + \frac{(c\hat{R})^2}{6} \quad (22)$$

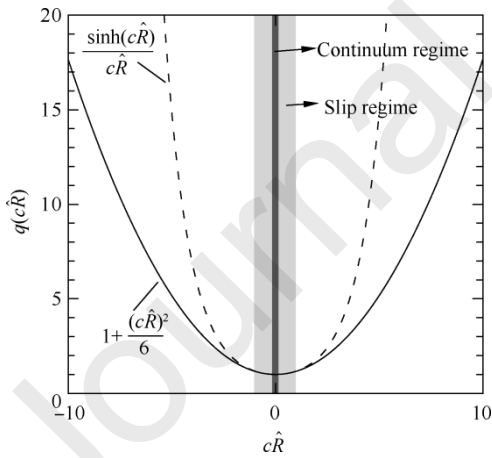


Fig. 1. Function curves of nonlinear factor $q(c\hat{R})$ and its truncated version.

As we can see from Fig. 1, for continuum and slip regimes, the truncated $q(c\hat{R})$ in Eq. (22) agrees well with the original $q(c\hat{R})$ in Eq. (21). Note that the truncated factor in Eq. (22) is acceptable only under moderate nonequilibrium conditions. According to Liu et al.⁵⁹, the nonlinear factor $q(c\hat{R})$ is overestimated

when $c\hat{R}$ is large, which would under-predict the numerical stress and heat flux. Therefore, with the above analytical simplification, the NCCR solvers for both normal and tangential directions mentioned in Section 2.2 can be re-written as below.

3.1. Compression and expansion solver

Substituting Eq. (15) and Eq. (22) into Eq. (14), we can obtain

$$\frac{c^2}{6} \left[\frac{3}{2} + \left(\frac{\hat{Q}_{x_i,0}}{\hat{I}_{x_i,x_i,0}^{u_{i,j}}} \right)^2 \right] \hat{I}_{x_i,x_i}^{u_{i,j}3} + (1 - \hat{I}_{x_i,x_i}^{u_{i,j}}) \hat{I}_{x_i,x_i}^{u_{i,j}} - \hat{I}_{x_i,x_i,0}^{u_{i,j}} = 0 \quad (23)$$

$$\hat{Q}_{x_i} = \frac{\hat{Q}_{x_i,0}}{\hat{I}_{x_i,x_i,0}^{u_{i,j}}} \hat{I}_{x_i,x_i}^{u_{i,j}} \quad (24)$$

Eq. (23) is a cubic equation with respect to $\hat{I}_{x_i,x_i}^{u_{i,j}}$, and we can show that there is a unique real root when $\hat{I}_{x_i,x_i}^{u_{i,j}} \hat{I}_{x_i,x_i,0}^{u_{i,j}} > 0$ is satisfied. Exact root exists for Eq. (23) (see Appendix A) and therefore the real roots of $\hat{I}_{x_i,x_i}^{u_{i,j}}$ can be found. After substituting $\hat{I}_{x_i,x_i}^{u_{i,j}}$ into Eq.(24), \hat{Q}_{x_i} is also obtained.

3.2. Shear flow solver

Likewise, after substituting Eqs. (18) and (22) into Eqs. (16) and (17), a quintic equation with respect to $\hat{I}_{x_i,x_i}^{u_{i,j}}$ can be derived

$$\begin{aligned} & \hat{I}_{x_i,x_i}^{u_{i,j}5} - 2\hat{I}_{x_i,x_i}^{u_{i,j}4} + \left(1 + \frac{4}{c^2}\right) \hat{I}_{x_i,x_i}^{u_{i,j}3} - \frac{4}{c^2} \hat{I}_{x_i,x_i}^{u_{i,j}2} \\ & + \frac{4}{c^4} \left(\frac{2\hat{I}_{x_i,x_i,0}^{u_{i,j}2}}{3} + 1 \right) \hat{I}_{x_i,x_i}^{u_{i,j}} + \frac{8\hat{I}_{x_i,x_i,0}^{u_{i,j}2}}{3c^4} = 0 \end{aligned} \quad (25)$$

However, there is no algebraic expression for the solutions of general quintic equations over the rationals. As a result, Eq. (25) cannot be solved analytically. Alternatively, an approximation method is introduced to obtain the solutions instead of conventional iterative methods. Specifically, combining Eqs. (16) and (17) yields

$$\hat{I}_{x_i,x_i}^{u_{i,j}2} = -\frac{3}{2} \hat{I}_{x_i,x_i}^{u_{i,j}} \left(\hat{I}_{x_i,x_i}^{u_{i,j}} + 1 \right) \geq 0 \quad (26)$$

through which we can further derive

$$-1 \leq \hat{I}_{x_i,x_i}^{u_{i,j}} \leq 0 \quad (27)$$

Therefore, our goal is to obtain an approximate

analytical solution on the interval $[-1, 0]$ for Eq. (25). According to Abel-Ruffini theorem⁶⁰, there is no solution in radicals to general polynomial equations of degree five or higher with arbitrary coefficients. Thus we can re-construct a quartic equation for $\hat{\Pi}_{x_i x_j}^{u_{j,i}5} - 2\hat{\Pi}_{x_i x_j}^{u_{j,i}4}$, the leading orders of Eq. (25), with the least-square method. Excellent agreement between the fitting polynomial $-2.904433x^4$ and $x^5 - 2x^4$ on the interval $[-1, 0]$ is found in Fig. 2. Finally, the approximate quartic equation on the interval $-1 \leq \hat{\Pi}_{x_i x_j}^{u_{j,i}} \leq 0$ is obtained as

$$\begin{aligned} & -2.904433\hat{\Pi}_{x_i x_j}^{u_{j,i}4} + \left(1 + \frac{4}{c^2}\right)\hat{\Pi}_{x_i x_j}^{u_{j,i}3} - \frac{4}{c^2}\hat{\Pi}_{x_i x_j}^{u_{j,i}2} \\ & + \frac{4}{c^4}\left(\frac{2\hat{\Pi}_{x_i x_j}^{u_{j,i}2}}{3} + 1\right)\hat{\Pi}_{x_i x_j}^{u_{j,i}} + \frac{8\hat{\Pi}_{x_i x_j}^{u_{j,i}2}}{3c^4} = 0 \end{aligned} \quad (28)$$

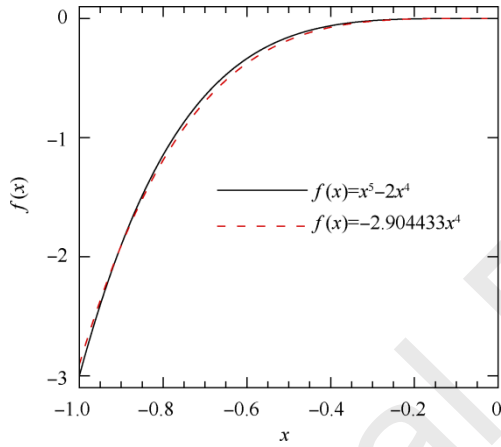


Fig. 2. Comparison between $x^5 - 2x^4$ and $-2.904433x^4$ on the interval $[-1, 0]$.

Similarly, it is shown that there is a unique real root for Eq. (28) if $-1 \leq \hat{\Pi}_{x_i x_j}^{u_{j,i}} \leq 0$. Exact root can be derived from Eq. (28) and the interested readers can see Appendix B for the detailed information.

3.3. Comparison with Myong's decomposed solver

In Sections 3.1 and 3.2, a new analytical method for decomposed NCCR system is proposed. Compared to the conventional iterative methods used for Myong's decomposed solver⁴², the analytical method is expected to be more efficient since the exact roots of the decomposed constitutive polynomials can be directly achieved. Meanwhile, it also preserves the nonlinear constitutive relations in the framework of the NCCR method.

To illustrate the different nonlinear properties of the analytical and iterative methods, the constitutive relations for compression and expansion as well as

shear flow problems ($c = 1.0179$) are respectively shown in Fig. 3 and Fig. 4. The N-S stresses from the linear constitutive relation are also added for comparison. In general, the solutions from the analytical method are close to those from Myong's decomposed solver for both normal and shear directions. They share the same mathematical properties as those of the solutions achieved through the iterative method for NCCR model by Myong⁴², i.e.

- (1) $\hat{\Pi}_{x_i x_j}^{u_{j,i}} = 0$ only when $\hat{\Pi}_{x_i x_j, 0}^{u_{j,i}} = 0$.
- (2) The unique solution $\hat{\Pi}_{x_i x_j}^{u_{j,i}}$ exists for all $\hat{\Pi}_{x_i x_j, 0}^{u_{j,i}}$.
- (3) The curve $\hat{\Pi}_{x_i x_j}^{u_{j,i}}(\hat{\Pi}_{x_i x_j, 0}^{u_{j,i}})$ is tangent to the Navier-Stokes curve $\hat{\Pi}_{x_i x_j}^{u_{j,i}} = \hat{\Pi}_{x_i x_j, 0}^{u_{j,i}}$ at $\hat{\Pi}_{x_i x_j, 0}^{u_{j,i}} = 0$.
- (4) $\hat{\Pi}_{x_i x_j}^{u_{j,i}} + 1 > 0$ is always true.
- (5) $d\hat{\Pi}_{x_i x_j}^{u_{j,i}} / d\hat{\Pi}_{x_i x_j, 0}^{u_{j,i}} \rightarrow 0$ when $\hat{\Pi}_{x_i x_j, 0}^{u_{j,i}} = \pm\infty$.

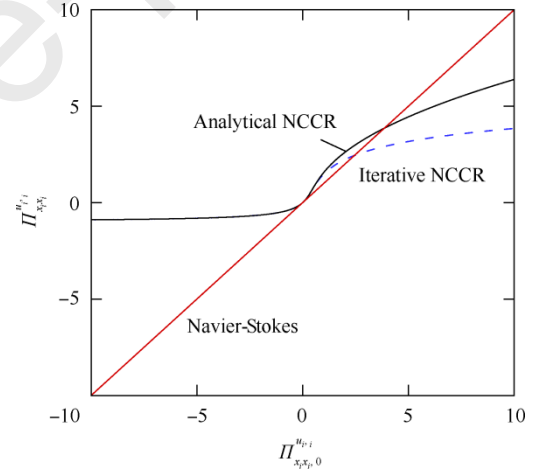


Fig. 3. Comparison of solutions from analytical and iterative method of NCCR model with N-S linear constitutive relation for compression and expansion problem ($c=1.0179$).

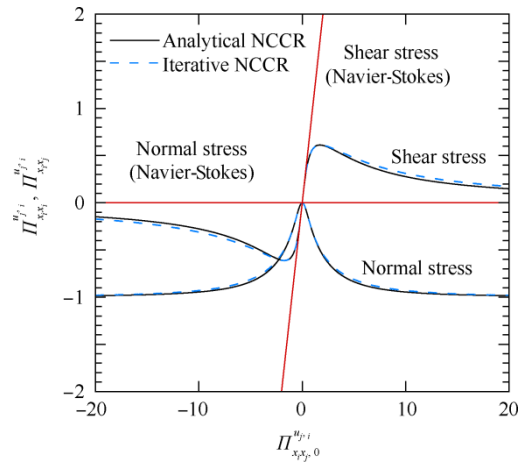
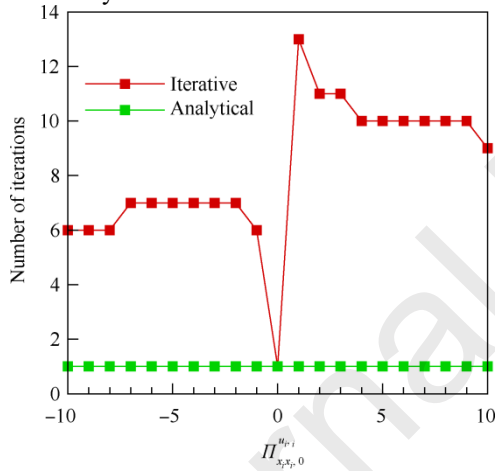


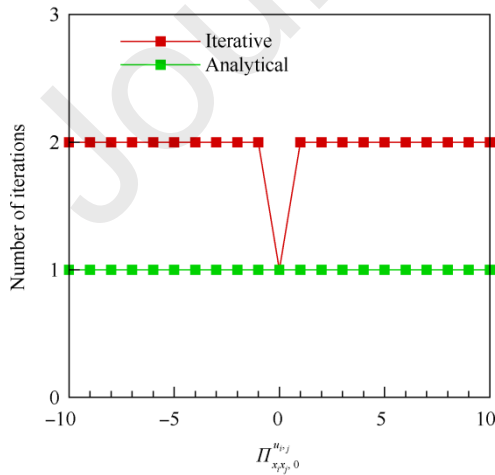
Fig. 4. Comparison of solutions from analytical and iterative methods with the N-S linear constitutive relation for shear flow problem ($c=1.0179$).

Moreover, Fig. 1 shows that the analytical method over-predicts the normal stress $\hat{\Pi}_{x_i x_i}^{u_{i,j}}$ when $\hat{\Pi}_{x_i x_i, 0}^{u_{i,j}}$ is larger than zero. It is shown that⁵⁹ the conventional NCCR model overestimates $q(c\hat{R})$ in prediction and large value of $q(c\hat{R})$ may lead to a dramatic decrease of stress and heat flux unphysically. However, the analytical method relieves this deficiency to some extent, which can be further confirmed by numerical cases in the next section.

Fig. 5 compares the number of iteration steps under different initial conditions for the iterative and analytical methods. Note that for the latter only one step is needed as shown in Fig. 5. For the iterative NCCR model, it generally takes at least 6-13 iterations for compression and expansion solver whilst takes 2 iterations for shear flow solver. Generally, the analytical method reduces total computational time considerably due to its non-iterative calculation.



(a) From compression and expansion solver



(b) From shear flow solver

Fig. 5. Computational cost of analytical and iterative NCCR methods.

3.4. Summary of analytical NCCR model

The entire essence of the analytical NCCR method is described in a detailed flowchart as shown in Fig.6. Briefly summarizing, Eu developed the generalized hydrodynamic equations from Boltzmann equation based on a nonequilibrium canonical distribution function and a cumulant expansion of the collisional integral³⁶, and next, with adiabatic assumption³⁶ and balanced closure⁴¹, NCCR model was developed. A decomposed nonlinear algebraic system of the NCCR model was then proposed by Myong, and by performing iterative method, the nonlinear algebraic system can be solved⁴². In this paper, by expanding the NCCR nonlinear factor around the equilibrium state and retaining the relevant terms until the second order of accuracy, we can solve the NCCR model with analytical method. Finally, we have the analytical NCCR method.

4. Results and discussion

In this section, several typical nonequilibrium flows, including shock wave structure (1D), Couette flow (quasi-1D), hypersonic flow past a cylinder (2D) and supersonic flow past a sphere (3D), are selected to validate the computational accuracy and stability of the proposed analytical NCCR method.

4.1. Shock wave structure of argon

The one-dimensional steady shock wave structure of argon gas is a benchmark case for validation of non-equilibrium models⁵⁸. The initial conditions in the upstream and downstream of shock wave can be determined by the Rankine–Hugoniot relations⁵⁸, i.e. (Note that the subscripts “0” and “1” indicate the states before and after the shock, respectively)

$$\begin{cases} \frac{\rho_1}{\rho_0} = \frac{u_0}{u_1} = \frac{(\gamma+1)Ma_0^2}{(\gamma-1)Ma_0^2+2} \\ \frac{p_1}{p_0} = 1 + \frac{2\gamma}{\gamma+1}(Ma_0^2-1) \\ \frac{T_1}{T_0} = \frac{[(\gamma-1)Ma_0^2+2](2\gamma Ma_0^2+1-\gamma)}{(\gamma+1)^2 Ma_0^2} \end{cases} \quad (29)$$

The dynamic viscosity of argon is estimated using the inverse power law⁵⁴, i.e.

$$\eta = \eta_{\text{ref}} \left(\frac{T}{T_{\text{ref}}} \right)^s \quad (30)$$

where T_{ref} , η_{ref} and s are reference temperature, reference dynamic viscosity and temperature exponent,

respectively. The properties of argon used in the computations are given in Table 2⁵⁸.

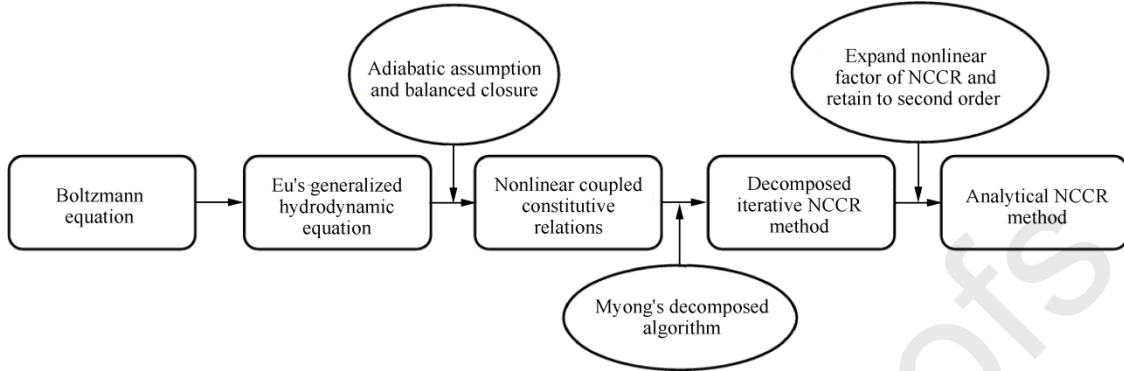


Fig. 6. Flowchart showing derivation process of analytical NCCR method

Table 2 Physical properties of argon⁵⁸.

Parameter	Pr	$R(\text{J} \cdot \text{kg}^{-1} \cdot \text{K}^{-1})$	γ	$T_{\text{ref}}(\text{K})$	$\eta_{\text{ref}}(\text{N} \cdot \text{s} \cdot \text{m}^{-2})$
Value	0.667	208	5/3	300	2.272×10^{-5}

In order to evaluate the performance of the analytical NCCR model, a series of test cases are investigated, which are characterized by different Mach numbers, ranging from $Ma = 1.2$ (the N-S equations are still valid) to 9.0 (the strong non-equilibrium effects are dominant).

Simulations based on Myong's iterative method and the developed analytical method are firstly conducted for the hard-sphere molecules at $Ma = 1.2, 2.0$ and 3.0. Ohwada's full Boltzmann equation solutions⁶¹ and N-S solutions are also added for comparison. The exponent s in Eq. (30) is assumed as 0.5 and the constant c in NCCR model is 1.1908⁵⁸. Fig. 7 shows the non-dimensional density, temperature, stress, and heat flux inside a shock layer for $Ma = 1.2, 2.0$ and 3.0. They respectively take the following forms:

$$\left\{ \begin{array}{l} \hat{\rho} = \frac{\rho}{\rho_0} \\ \hat{T} = \frac{T}{T_0} \\ \hat{\tau}_{xx} = \frac{\tau_{xx}}{p_0} \\ \hat{q}_x = \frac{q}{\rho_0 (2RT)^{3/2} / 2} \end{array} \right. \quad (31)$$

where the quantities with subscript "0" represent the upstream parameters of the shock wave. The horizontal axis is normalized by mean free path l_0 . In Fig. 7(a), with $Ma = 1.2$, both NCCR and Boltzmann solutions are almost the same as N-S results since the flow is not far from equilibrium. As the Mach number increases to 2.0 and 3.0, the NCCR model performs better than the N-S equations when both solutions are compared to the Boltzmann counterparts, especially in shock rising position. Moreover, the results of the analytical NCCR model are close to those from the NCCR iterative method, which indicates that the approximation of the analytical algorithm is reasonable in the calculation of one-dimensional shock wave structure and it has nearly the same performance with the iterative model under the studied Mach number conditions.

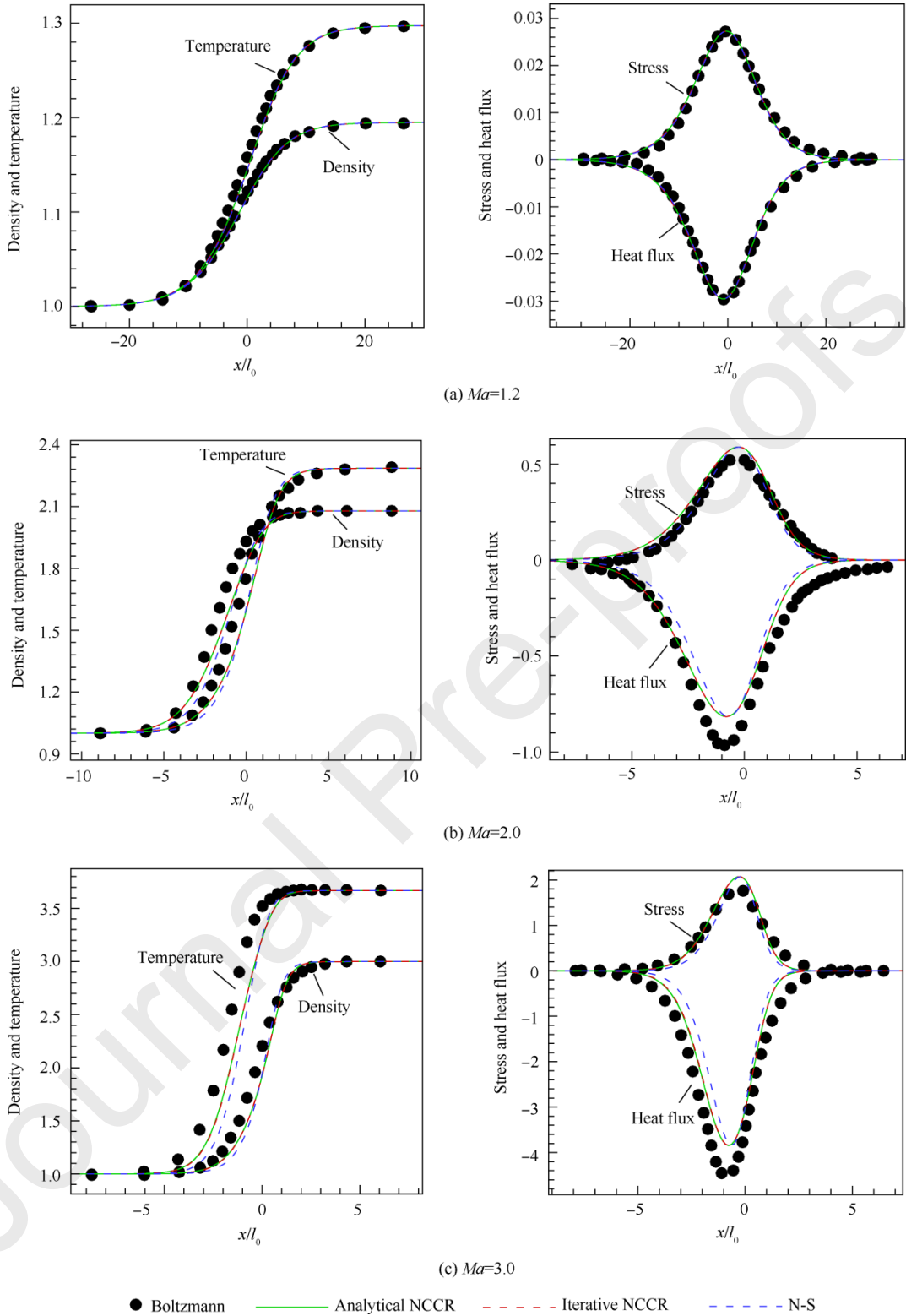


Fig. 7. Comparison of analytical and iterative NCCR models for argon shock waves

The shock wave structure of argon at higher Mach numbers, i.e. $Ma = 8.0$ and 9.0 , are investigated based on the two NCCR models. The exponent s in Eq.(30) is assumed as 0.72 and the constant c in the NCCR model

is 1.0179^{58} . The solutions of the non-dimensional density, temperature, stress and heat flux inside a shock layer are shown in Fig. 8, and the solutions evaluated by Bird's 1D DSMC code⁶² and experimental

measurements^{63, 64} are also presented for reference. The scaled density and temperature are obtained through

$$\hat{\rho} = \frac{\rho - \rho_0}{\rho_1 - \rho_0}, \quad \hat{T} = \frac{T - T_0}{T_1 - T_0} \quad (32)$$

where the quantities with subscript “1” represent the downstream parameters of the shock wave. Stress and heat flux are normalized with Eq.(31). The maximum gradient-length local Knudsen number, which is proposed by Boyd et al. as a continuum breakdown parameter^{65, 66}, is introduced to describe the degree of non-equilibrium state, i.e.

$$Kn_{\text{GLL}} = \frac{l}{Q} \left| \frac{dQ}{dl} \right| \quad (33)$$

where l is the mean free-path and Q is a variable of interest, such as density, temperature or pressure. Higher value of Kn_{GLL} represents higher degree of non-equilibrium. Based on Fig. 8, Kn_{GLL} reaches its peak value at upstream region of shock wave (i.e.

$x/l_0 \approx -3$), where the strong non-equilibrium effect exists. In the upstream region of shock wave, the results from our analytical method are closer to the DSMC and experimental results than the iterative method results, whose shock profiles rise later. In addition, the underestimation of both stress and heat flux in the iteration NCCR model is observed in the upstream region and the analytical method alleviates it to some degree. This may be due to the fact that the original nonlinear factor $q(c\hat{R})$ of NCCR model is not quite physical in very strong non-equilibrium regimes⁵⁹. In the downstream region of the shock wave where the non-equilibrium effect is relatively weak (i.e. smaller Kn_{GLL}), the results from the iterative and analytical methods are similar. As we noted earlier, DSMC has been used as a standard, and Fig.8 shows that DSMC results agree with the experimental data very well. Moreover, there are limited experiments in low-density monatomic gas flows. Hence, DSMC simulations will serve as benchmarks for the following cases.

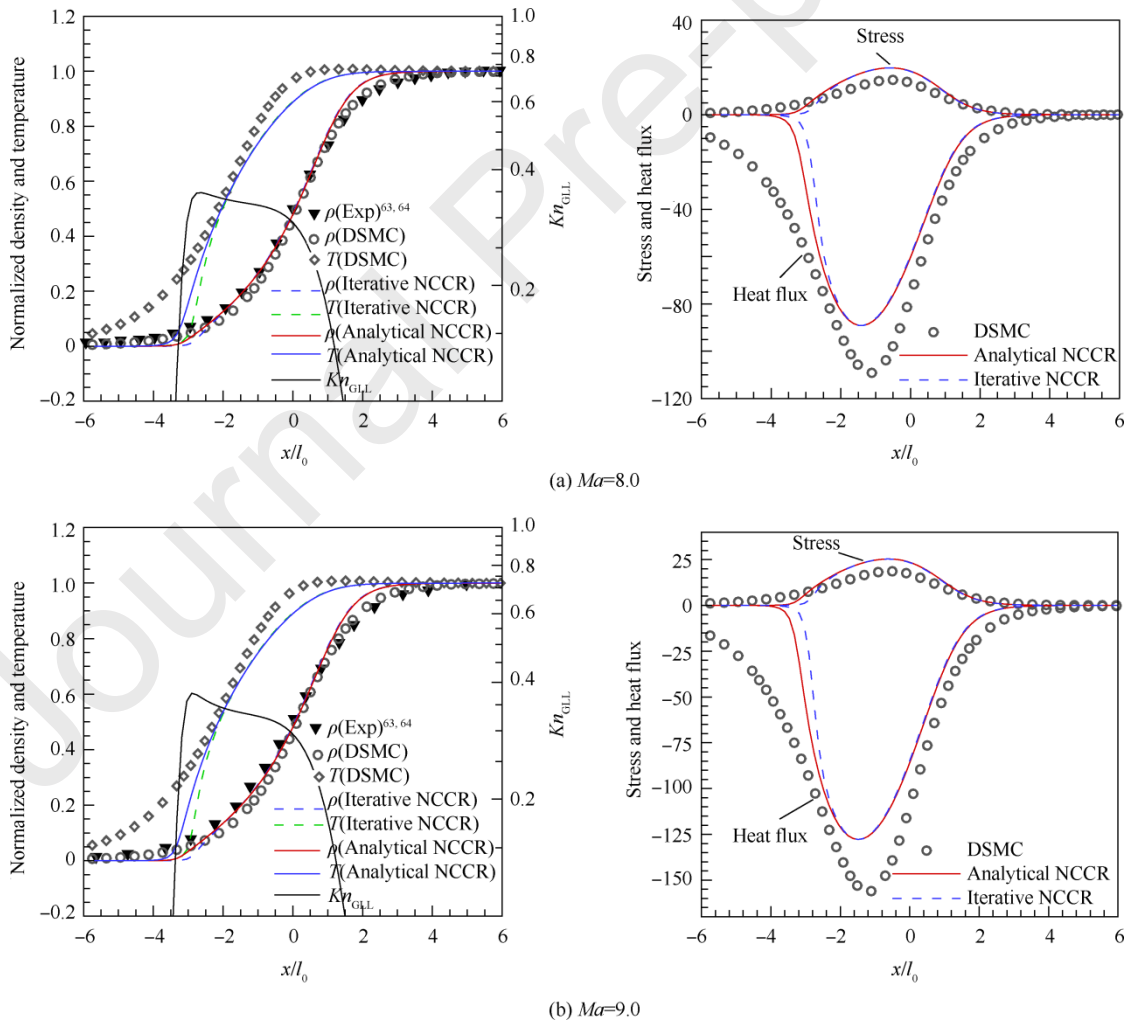


Fig. 8. Comparison of analytical and iterative NCCR models for argon shock wave (DSMC results are evaluated with Bird’s 1D DSMC code⁶²).

4.2. Couette flow

Here the Couette flow problem⁶⁷ is selected to examine the capability of the analytical NCCR method for low-speed flows. The Couette flow is driven by two infinite flat plates moving parallel to opposite directions with constant speed u_0 . The temperature of each wall is T_w and the distance between the two flat plates is L . The global Knudsen number is used to represent the degree of non-equilibrium effect⁶⁷, i.e.

$$Kn = l_0 / L \quad (34)$$

Here $u_0 = 50$ m/s and $T_w = 273$ K are adopted, while L is varied based on different Knudsen numbers. Enhanced NCCR-based slip boundary conditions proposed by Jiang et al.⁵⁷ are adopted for the walls, which read

$$\begin{aligned} u - u_w &= \frac{2 - \sigma_u}{\sigma_u} \left(\frac{l}{-\eta} \Pi_{\text{NCCR}} + \frac{l^2}{2\eta} \cdot \frac{\partial \Pi_{\text{NCCR}}}{\partial y} \right) \\ T - T_w &= \frac{2 - \sigma_T}{\sigma_T} \cdot \frac{2\gamma}{(\gamma + 1)Pr} \left(\frac{l}{-\lambda} Q_{y,\text{NCCR}} + \frac{l^2}{2\lambda} \cdot \frac{\partial Q_{y,\text{NCCR}}}{\partial y} \right) \end{aligned} \quad (35)$$

The subscript w indicates the quantities of the wall. Π_{NCCR} denotes the tangential shear stress along the surface and $Q_{y,\text{NCCR}}$ denotes the heat flux perpendicular to the surface. They are both calculated from the analytical NCCR method. $\sigma_u = 1.0$ and $\sigma_T = 1.0$ are used in the following cases.

In order to keep the numerical stability, a relaxation method is used to obtain the velocity slip and temperature jump at the walls⁶⁷,

$$\begin{cases} u_s^r = u_s^n + R_f (u_s^{n+1} - u_s^n) \\ T_j^r = T_j^n + R_f (T_j^{n+1} - T_j^n) \end{cases} \quad (36)$$

Here R_f is the relaxation factor and is set to be 2.0×10^{-6} suggested by Jiang et al.⁵⁷ Argon is used to simulate the Couette flow. The exponent s in Eq.(30) is assumed as 0.75 and the constant c in the NCCR model is 1.0179⁴².

Fig. 9 shows the velocity distribution of Couette flow predicted by different methods for $Kn = 0.012, 0.10, 0.25, 0.50, 0.75$ and 1.00. They represent different non-equilibrium situations from continuum regime to transition regime. The DSMC and R13 results by Refs.^{24, 68} are also demonstrated for comparison. At $Kn = 0.012$ and 0.1, Figs. 9(a) and 9(b) show that the velocity profiles predicted with R13, analytical NCCR method and N-S equations are in excellent agreement with the DSMC results. As the Knudsen number

increases, the predicted velocity profiles of the foregoing methods show pronounced difference from those from the DSMC approach, which indicate an underlying non-equilibrium phenomenon in the micro-Couette flow. Weakly nonlinear velocity profiles can be observed in Figs. 9(d)-9(f), where all the models fail to capture except DSMC. However, the velocity profiles predicted by analytical NCCR method and the R13 model are closer to DSMC results than those by N-S equations. The profiles obtained by the analytical NCCR are very close to those by the R13 model, even though R13 model is the evolution equations of 13 moments and the analytical NCCR method is much simpler evolution equations of 5 moments.

The temperature distribution of Couette flow predicted by different methods is shown in Fig. 10. As can be seen from Figs. 10(d)-10(f), the linear N-S equations with first-order Maxwell slip boundary conditions do not capture the non-equilibrium effects at walls for Knudsen number above 0.5. The R13 and NCCR profiles are closer to the DSMC results than the linear N-S results, although their results start to diverge from the DSMC profiles at $Kn = 0.25$, where the R13 overestimates and the NCCR model underestimates the temperature in the central region of the Couette flow. For $Kn \geq 0.5$, the temperature decrease predicted by the analytical NCCR method is much closer than those of the R13 and N-S. However, the limitation of the analytical NCCR method is also shown in the central regions for Knudsen number above 0.1, because it gives lower temperature at these regions. The behavior of the analytical NCCR method is more like the linear NS equations in these regions, but it performs better at walls and gives better temperature jump values than the R13 and the N-S equations when compared to the DSMC results.

Since a better performance of the analytical NCCR method is shown in the above results, its capability still deserves to be investigated more carefully. The normal heat flux and shear stress distribution of Couette flow predicted by different methods over a range of Knudsen numbers from 0.1 to 1.0 are shown in Fig. 11. Because of the symmetry of the flow field in Couette flow, only the upper-half distribution of the heat flux and shear stress profiles is plotted. At $Kn = 0.1$, normal heat flux and shear stress from all the methods agree well with the DSMC results. However, with increased Knudsen number, the degree of nonequilibrium increases. Difference arises among the results from different methods. In the transition regime, Fig. 11 presents constant shear stresses across the domain for the planar Couette flow. The deviation between the three continuum-based hydrodynamic models and the DSMC method increases as the flow deviates from the thermal equilibrium with about 7% overestimation at $Kn = 0.25, 0.5$ and 9% overestimation at $Kn = 1.0$. For normal heat flux, the results predicted by the linear N-S

equations deviate from the DSMC results for $Kn > 0.1$. However, both the R13 and analytical NCCR methods show fairly good agreement with the DSMC results for $Kn < 1.0$, except for the nonlinear behavior near the wall. For $Kn = 1.0$, all the three continuum-based

hydrodynamic models deviate from the DSMC results, but the R13 and the analytical NCCR methods perform much better than the N-S equations.

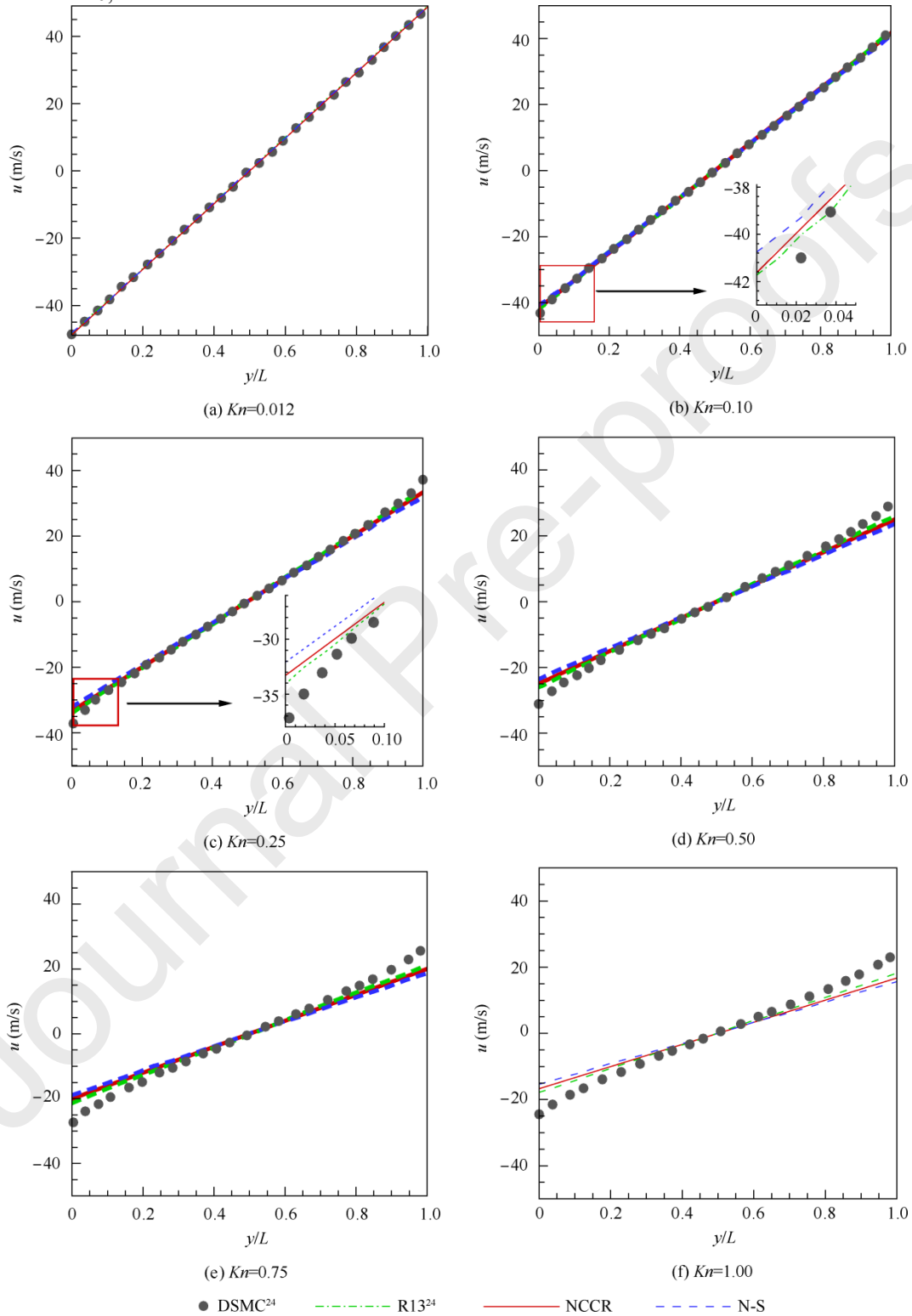


Fig. 9. Velocity distribution of Couette flows predicted by different methods over a range of Knudsen numbers.

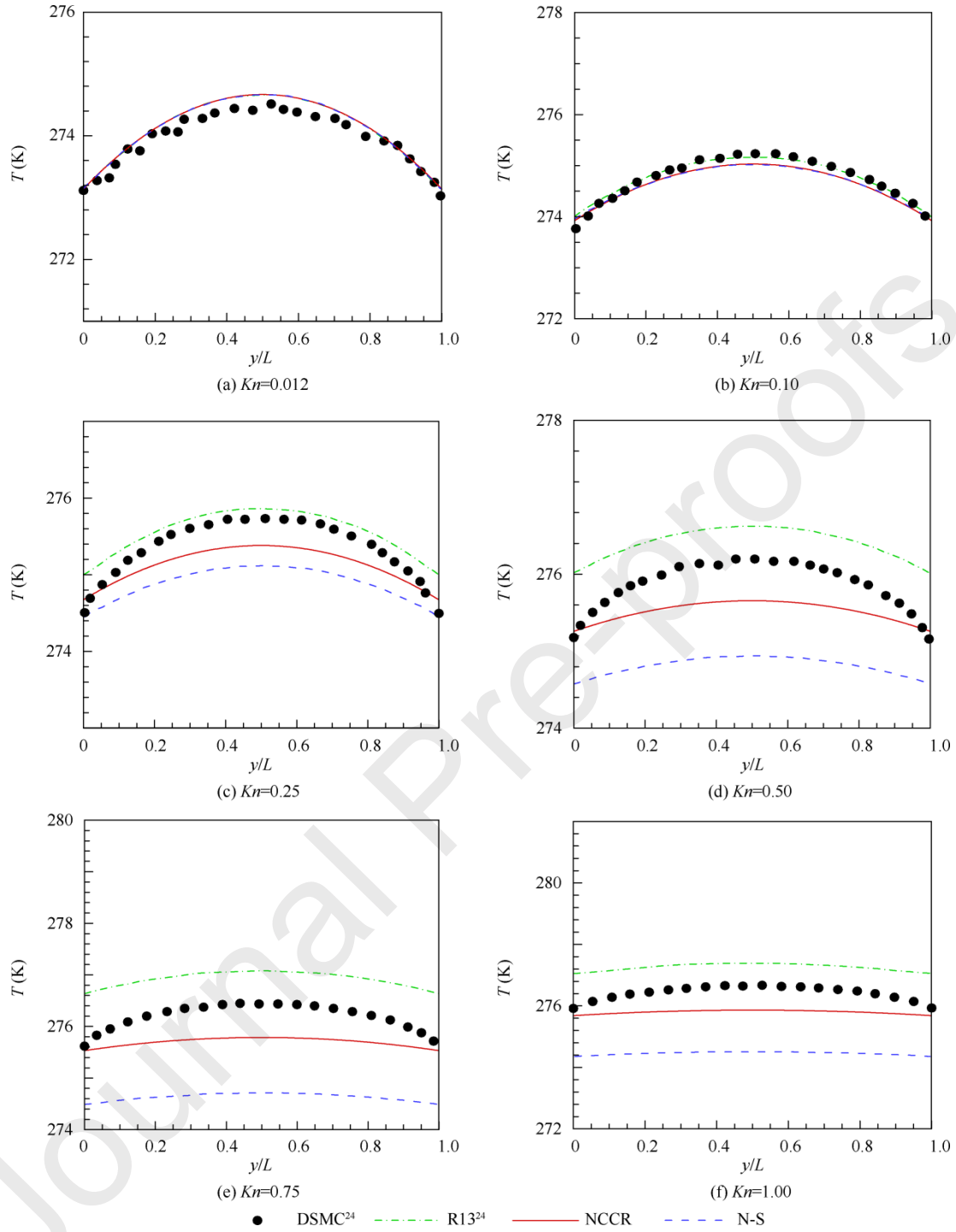


Fig. 10. Temperature distribution of Couette flow predicted by different methods over a range of Knudsen numbers.

4.3. A hypersonic flow around a 2D cylinder for argon gas

The analytical method is further validated for argon gas flows around a 2D cylinder with radius of 0.1524 m where $Ma = 10$ and $Kn = 0.004, 0.02, 0.1$ (The

characteristic length is the radius of the cylinder). The free-stream conditions are taken from Ref.⁶⁶, where corresponding densities of the free-stream gas are 1.408×10^{-4} , 2.818×10^{-5} and 5.636×10^{-6} . The first-order Maxwell slip boundary condition is applied at the wall surface and other calculation parameters are shown in Table 3.

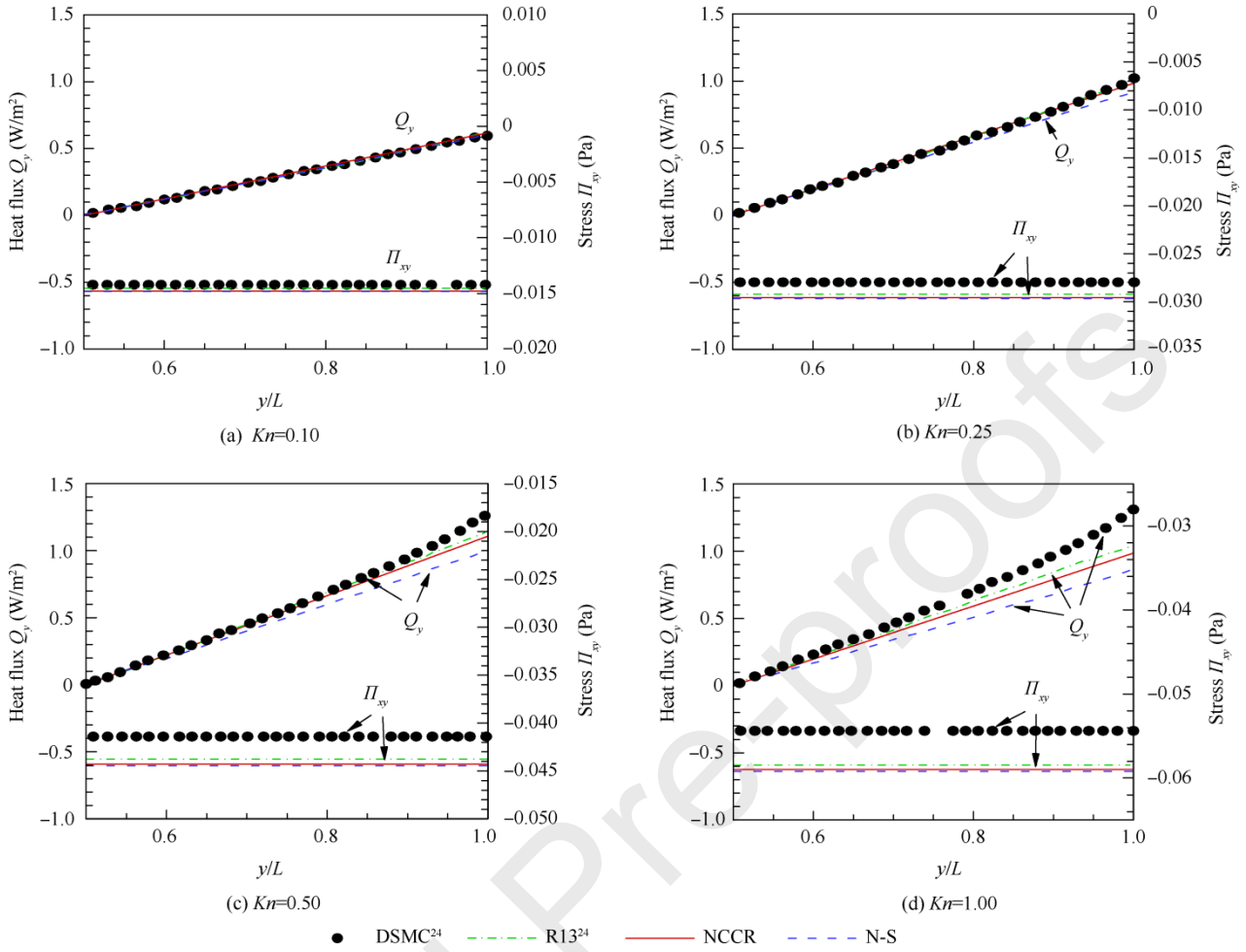


Fig. 11. Normal heat flux and shear stress distribution of Couette flow predicted by different methods over a range of Knudsen numbers.

Table 3 Calculation parameters for hypersonic flow past a cylinder.

Parameter	U_∞ (m·s ⁻¹)	T_∞ (K)	T_w (K)	Pr	c	γ	R (J·kg ⁻¹ ·K ⁻¹)	T_{ref} (K)	η_{ref} (N·s·m ⁻²)	s
Value	2624	200	500	2/3	1.0179	5/3	208.16	1000	5.081×10^{-5}	0.734

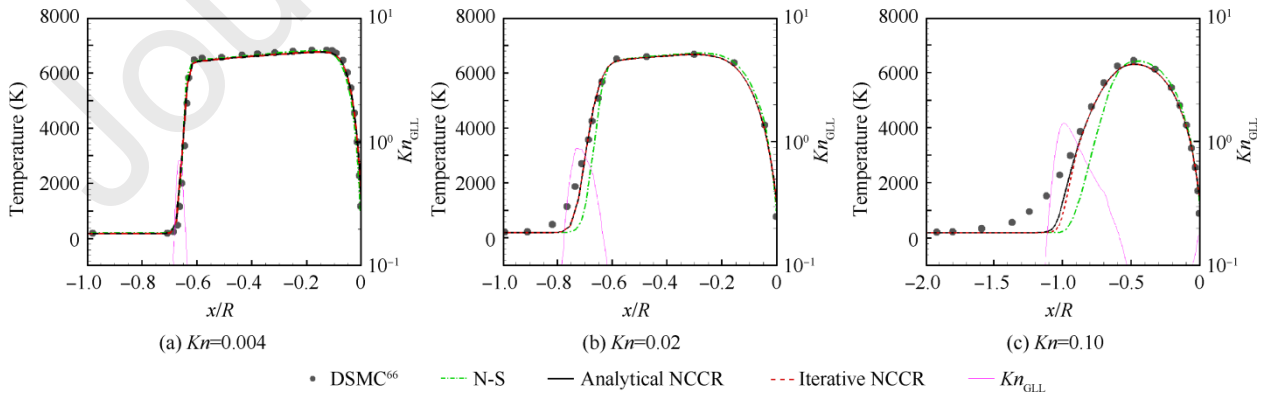


Fig. 12. Temperature and maximum gradient-length local Knudsen number Kn_{GLL} along the stagnation line of $Ma = 10$ cylinder at different Kn

Since the prediction of the temperature profile is more difficult than those of density, velocity, and pressure, only the temperature on the stagnation line is presented in Refs.^{59, 66} Therefore, only the temperature predicted from different methods are shown in Fig. 12. Gradient-length local Knudsen number (Kn_{GLL}) of each case is also plotted for comparison. Continuum hypothesis is not valid if Kn_{GLL} is greater than 0.05⁶⁶. Therefore, the non-equilibrium effect needs to be taken into account inside the shock at each case.

At $Kn = 0.004$, which corresponds to the continuum flow regime, the temperature profiles predicted by N-S and NCCR are close to the DSMC solution. Nevertheless, at $Kn = 0.02$, which belongs to the slip flow regime, the results from different constitutive relations start to deviate from that of the DSMC, especially at regions inside shock wave where Kn_{GLL} is higher. Both of the two NCCR methods yield better results than the N-S constitutive relations, and they provide almost the same results. Moreover, at $Kn = 0.1$, which is in the transitional flow regime, both methods are better than N-S equations. It should be highlighted that the analytical method provides even better results than iterative one although it is an approximation of NCCR for the situation which is not far from the equilibrium. It indicates that the analytical method is a reliable and efficient way to solve those far-from-equilibrium flows.

The computational efficiency of analytical method and iterative method is investigated based on the same computer infrastructure. The average computation time

per step of cases above for 10000 steps at 11,440 structured grids is listed in Table 4. About 1/3 of the computation time on average is saved for these cases in the calculation of the inviscid flux and other computational overhead. It can be expected that more pronounced speed-up can be achieved when complex geometries discretized with millions of grids are considered.

Table 4 Computation time per step of each selected case.

Kn	Computation time (ms)	
	0.004	Analytical
	Iteration	58.7
0.02	Analytical	76.0
	Iteration	101.6
0.1	Analytical	73.5
	Iteration	112.8

4.4. A supersonic flow around a 3D sphere for argon gas

The analytical NCCR method is validated for monatomic gas flows around a 3D sphere with a radius of 1.9 mm in slip regime. Compared to the two-dimensional case in Section 4.3, here we would like to examine the ability of the analytical NCCR method in predicting 3D problems. The monatomic gas is assumed argon with $s=0.75$ in the inverse power law and $c=1.0179$. The inflow parameters are given in Table 5.

Table 5 Calculation parameters for supersonic flow past a sphere.

Parameter	Ma_∞	T_∞ (K)	Kn_∞	p_∞ (Pa)	T_w (K)	Pr	γ	R (J·kg ⁻¹ ·K ⁻¹)	T_{ref} (K)	η_{ref} (N·s·m ⁻²)
Value	3.5	26.6	0.05	5	135.27	2/3	5/3	208.16	1000	5.081×10^{-5}

To reduce the computational cost, a quarter of the computational domain is considered in this work. Typical structured grids of the computational domain are demonstrated in Fig. 13 with 80 nodes in the radial direction of the sphere. First-order Maxwell slip boundary condition is applied at the solid surface. DSMC result is calculated with opensource code Spartan⁶⁹ as a benchmark. Fig. 14 shows the maximum gradient-length-local Knudsen number computed by the analytical NCCR method. It can be seen from the contour of Kn_{GLL} that the continuum hypothesis is not valid inside the stand-off shock and near the solid surface of the rear of the sphere, where Kn_{GLL} exceeds the critical value of 0.05. It is generally believed that N-S equation cannot obtain accurate predictions in these regions.

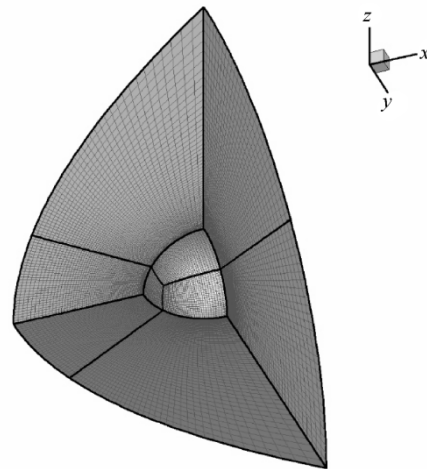


Fig. 13. Structured cell distribution.

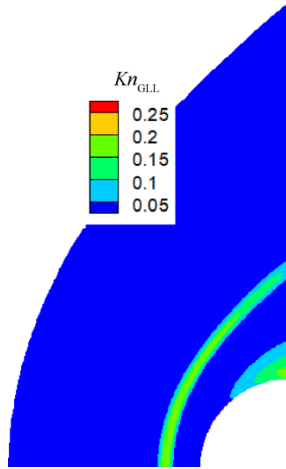


Fig. 14. Contour of gradient length local Knudsen number.

Comparison of the density and temperature between N-S equation and the analytical NCCR method is made in Fig. 15 and Fig. 16, respectively. It is shown that the shock thickness predicted by the analytical NCCR method is slightly thicker than that by the N-S equation. Also, the shock stand-off distance is larger from the analytical NCCR method compared to the N-S equation. These predictions agree with each other in terms of the Kn_{GLL} distribution in Fig. 14 as the flow regions inside the shock wave are far from the thermodynamic equilibrium. Also, the normalized temperature and density distribution along the normalized stagnation line evaluated by DSMC, N-S and the analytical NCCR method are plotted for further analysis in Fig. 15 and Fig. 16. One feature which should be highlighted is that the analytical NCCR method shows better agreement with DSMC data in terms of density and temperature at the stagnation line. Nevertheless, there are still some differences between DSMC and the analytical NCCR method near the shock wave. It may imply that some key features are not included in the analytical NCCR method when it is simplified from Eu's generalized hydrodynamic equations.

5. Conclusions

To overcome the deficiency of traditional iterative method in solving NCCR model, an analytical method is proposed by expanding and truncating the nonlinear factor in decomposed solvers to predict nonequilibrium rarefied flows. Without iterative procedure, analytical method is more efficient and preserves the capability of describing non-equilibrium flows in NCCR. To validate its efficiency and accuracy, numerical cases including one-dimensional shock wave structures, Couette flow, two-dimensional hypersonic flows around a cylinder and three-dimensional supersonic flow around a sphere are employed. The results of these cases show that both analytical method and iterative method yield better

agreement with experimental and DSMC data in non-equilibrium flows compared with continuum N-S equations. More importantly, the non-iterative feature of the proposed analytical method reduces the computational time considerably in both decomposed solvers, which could make NCCR method be a promising engineering tool for modelling rarefied non-equilibrium flows.

Acknowledgements

This work was financially supported by the National Natural Science Foundation of China (Nos.: 11502232, 51575487, 11572284, and 6162790014). Zhiqiang HE gratefully acknowledges the support by the China Scholarship Council (No. 201906320279). The computational work for this article was partially performed on resources of the National Supercomputing Centre, Singapore (<https://www.nsc.sg>).

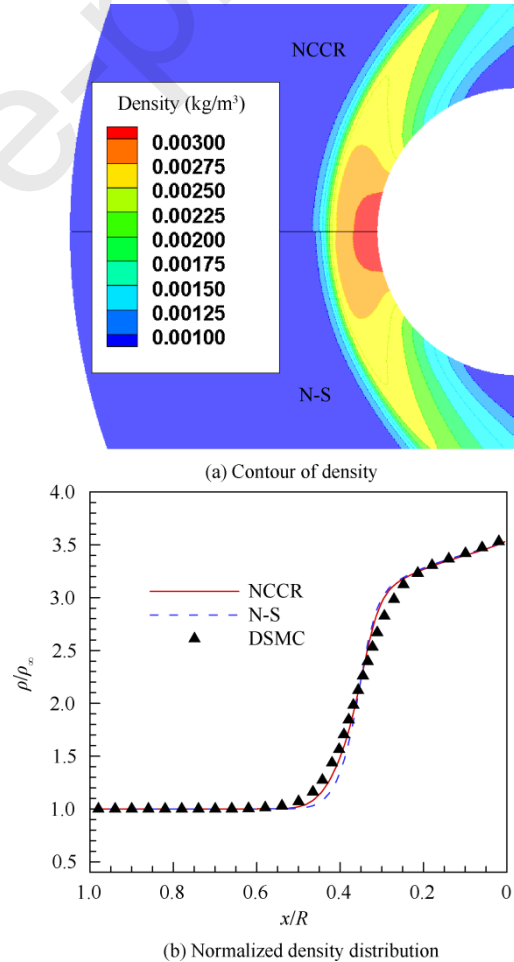


Fig. 15. Contour of density and normalized density distribution along normalized stagnation line predicted by N-S equations and analytical NCCR method (DSMC result is calculated with opensource code Spartan⁶⁹).

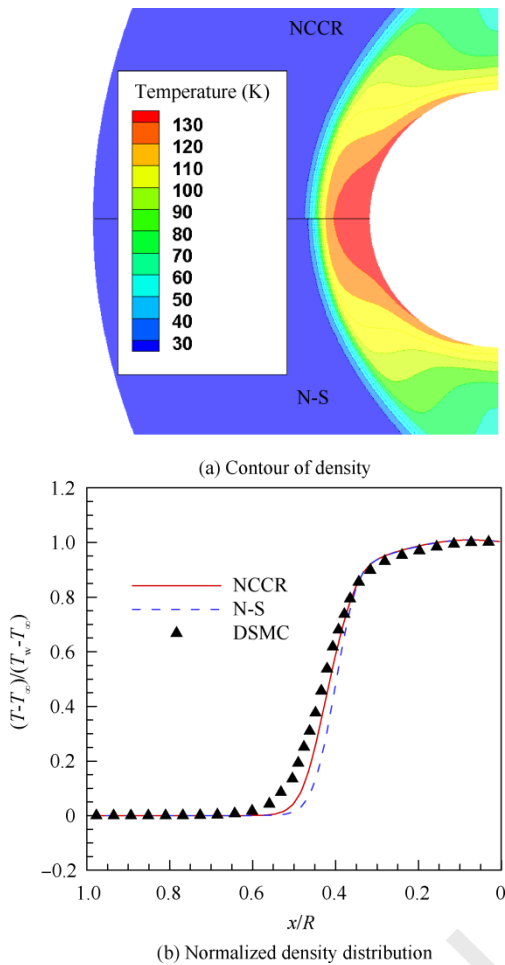


Fig. 16. Contour of temperature and normalized temperature distribution along normalized stagnation line predicted by N-S equations and analytical NCCR method (DSMC result is calculated with opensource code Spartán⁶⁹)

References

1. Tsien HS. Superaerodynamics, mechanics of rarefied gases. *Journal of the Aeronautical Sciences* 1946; 13(12):653-64.
2. Bai C, Li J, Li S, et al. Review of theoretical achievements for starting flow problem for all mach numbers. *Chinese Journal of Aeronautics* 2019; 32(1):78 - 91.
3. Sun X, Huang W, Ou M, et al. A survey on numerical simulations of drag and heat reduction mechanism in supersonic/hypersonic flows. *Chinese Journal of Aeronautics* 2019; 32(4):771 - 84.
4. Li Z, Xia X, Li X, et al. Numerical exploration on the thermal invasion characteristics of two typical gap-cavity structures subjected to hypersonic airflow. *Chinese Journal of Aeronautics* 2020.
5. Yang J, Liu M. Numerical analysis of hypersonic thermochemical non-equilibrium environment for an entry configuration in ionized flow. *Chinese Journal of Aeronautics* 2019; 32(12):2641 - 54.
6. Guo J, Lin G, Bu X, Li H. Sensitivity analysis of flowfield modeling parameters upon the flow structure and aerodynamics of an opposing jet over a hypersonic blunt body. *Chinese Journal of Aeronautics* 2020; 33(1):161 - 75.
7. Bird G. *Molecular gas dynamics and the direct simulation of gas flows*. Oxford: Clarendon Press; 1994.
8. Bird GA. Aspects of the structure of strong shock waves. *Physics of Fluids* 1970; 13(5):1172-7.
9. Sharipov F. *Discrete velocity method. Rarefied gas dynamics*. New York: John Wiley & Sons, Ltd; 2015.p.83-96.
10. Broadwell JE. Study of rarefied shear flow by the discrete velocity method. *Journal of Fluid Mechanics* 1964; 19(3):401-14.
11. Wu L, Reese JM, Zhang Y. Solving the boltzmann equation deterministically by the fast spectral method: Application to gas microflows. *Journal of Fluid Mechanics* 2014; 746:53-84.
12. Xu K, Huang JC. An improved unified gas-kinetic scheme and the study of shock structures. *IMA Journal of Applied Mathematics* 2011; 76(5):698-711.
13. Xu K, Huang JC. A unified gas-kinetic scheme for continuum and rarefied flows. *Journal of Computational Physics* 2010; 229(20):7747-64.
14. Xu K. *Direct modeling for computational fluid dynamics: Construction and application of unified gas-kinetic schemes*. Singapore: World Scientific; 2015.
15. Guo Z, Xu K, Wang R. Discrete unified gas kinetic scheme for all knudsen number flows: Low-speed isothermal case. *Phys Rev E Stat Nonlin Soft Matter Phys* 2013; 88(3):033305.
16. Zhu L, Guo Z, Xu K. Discrete unified gas kinetic scheme on unstructured meshes. *Computers & Fluids* 2016; 127:211-25.
17. Li ZH, Zhang HX. Study on gas kinetic unified algorithm for flows from rarefied transition to continuum. *Journal of Computational Physics* 2004; 193(2):708-38.
18. Li ZH, Peng AP, Zhang HX, et al. Rarefied gas flow simulations using high-order gas-kinetic unified algorithms for boltzmann model equations. *Progress in Aerospace Sciences* 2015; 74:81-113.
19. Peng AP, Li ZH, Wu JL, et al. Implicit gas-kinetic unified algorithm based on multi-block docking grid for multi-body reentry flows covering all flow regimes. *Journal of Computational Physics* 2016; 327:919-42.
20. Balakrishnan R, Agarwal RK, Yun KY. Bgk-burnett equations for flows in the continuum-transition regime. *Journal of Thermophysics and Heat Transfer* 1999; 13(4):397-410.
21. Singh N, Agrawal A. Onsager's-principle-consistent 13-moment transport equations. *Phys Rev E* 2016; 93(6):063111.
22. Zhao W, Chen W, Agarwal RK. Formulation of a new set of simplified conventional burnett equations for computation of rarefied hypersonic flows. *Aerospace Science and Technology* 2014; 38:64-75.
23. Torrilhon M, Struchtrup H. Regularized 13-moment equations: Shock structure calculations and comparison to burnett models. *Journal of Fluid Mechanics* 2004; 513:171-98.
24. Gu XJ, Emerson DR. A high-order moment approach for capturing non-equilibrium phenomena in the transition regime. *Journal of Fluid Mechanics* 2009; 636:177-216.

25. Grad H. On the kinetic theory of rarefied gases. *Communications on Pure and Applied Mathematics* 1949; 2(4):331-407.
26. McDonald J, Torrilhon M. Affordable robust moment closures for cfd based on the maximum-entropy hierarchy. *Journal of Computational Physics* 2013; 251:500-23.
27. Cai Z, Fan Y, Li R. Globally hyperbolic regularization of grad's moment system. *Communications on Pure and Applied Mathematics* 2014; 67(3):464-518.
28. Struchtrup H. *Macroscopic transport equations for rarefied gas flows*. Berlin: Springer; 2005..
29. Burnett D. The distribution of molecular velocities and the mean motion in a non-uniform gas. *Proceedings of the London Mathematical Society* 1936; s2-40(1):382-435.
30. Grad H. The profile of a steady plane shock wave. *Communications on Pure and Applied Mathematics* 1952; 5(3):257-300.
31. Weiss W. Continuous shock structure in extended thermodynamics. *Physical Review E* 1995; 52(6):R5760-R3.
32. Zhao W, Chen W, Liu H, et al. Computation of 1-d shock structure in a gas in rotational non-equilibrium using a new set of simplified burnett equations. *Vacuum* 2014; 109:319-25.
33. Holway LH. Existence of kinetic theory solutions to the shock structure problem. *Physics of Fluids* 1964; 7(6):911-3.
34. Gu XJ, Emerson DR, Tang GH. Kramers' problem and the knudsen minimum: A theoretical analysis using a linearized 26-moment approach. *Continuum Mechanics Thermodynamics* 2009; 21(5):345.
35. Eu BC. *Nonequilibrium statistical mechanics*. Netherlands: Springer Science & Business Media; 1998.
36. Eu BC. *Kinetic theory of nonequilibrium ensembles, irreversible thermodynamics, and generalized hydrodynamics*. Switzerland: Springer; 2016.
37. Eu BC, Al-Ghoul M. *Chemical thermodynamics*. 2nd ed. Singapore: World Scientific; 2018.
38. Eu BC. A modified moment method and irreversible thermodynamics. *The Journal of Chemical Physics* 1980; 73(6):2958-69.
39. Al-Ghoul M, Eu B. Generalized hydrodynamics and shock waves. *Physical Review E* 1997; 56(3):2981-92.
40. Eu BC, Ohr YG. Generalized hydrodynamics, bulk viscosity, and sound wave absorption and dispersion in dilute rigid molecular gases. *Physics of Fluids* 2001; 13(3):744-53.
41. Myong RS. On the high mach number shock structure singularity caused by overreach of maxwellian molecules. *Physics of Fluids* 2014; 26(5):056102.
42. Myong RS. Thermodynamically consistent hydrodynamic computational models for high-knudsen-number gas flows. *Physics of Fluids* 1999; 11(9):2788-802.
43. Myong RS. A computational method for eu's generalized hydrodynamic equations of rarefied and microscale gasdynamics. *Journal of Computational Physics* 2001; 168(1):47-72.
44. Myong RS. A generalized hydrodynamic computational model for rarefied and microscale diatomic gas flows. *Journal of Computational Physics* 2004; 195(2):655-76.
45. Myong RS. Coupled nonlinear constitutive models for rarefied and microscale gas flows: Subtle interplay of kinematics and dissipation effects. *Continuum Mechanics and Thermodynamics* 2009; 21(5):389-99.
46. Myong RS. A full analytical solution for the force-driven compressible poiseuille gas flow based on a nonlinear coupled constitutive relation. *Physics of Fluids* 2011; 23(1):012002.
47. Xiao H, Myong R, Singh S. A new near-equilibrium breakdown parameter based on the rayleigh-onsager dissipation function. *AIP conference proceedings*. 2014.
48. Myong RS. Numerical simulation of hypersonic rarefied flows using the second-order constitutive model of the boltzmann equation. *Advances in some hypersonic vehicles technologies: IntechOpen*; 2018.
49. Le NTP, Xiao H, Myong RS. A triangular discontinuous galerkin method for non-newtonian implicit constitutive models of rarefied and microscale gases. *Journal of Computational Physics* 2014; 273:160-84.
50. Xiao H, Shi Y, Shang Y, et al. Validation of nonlinear coupled constitutive relations in near-equilibrium gas flows. *Manned Spaceflight* 2015; (3):18.
51. Xiao H, Tang K. A unified framework for modeling continuum and rarefied gas flows. *Sci Rep* 2017; 7(1):13108.
52. Jiang Z, Chen W, Zhao W. A new coupled computational method in conjunction with three-dimensional finite volume schemes for nonlinear coupled constitutive relations. *arXiv preprint arXiv:161101281* 2016.
53. Jiang Z, Zhao W, Chen W. A three-dimensional finite volume method for conservation laws in conjunction with modified solution for nonlinear coupled constitutive relations. *AIP conference proceedings*. 2016.
54. Jiang Z. An undecomposed hybrid algorithm for nonlinear coupled constitutive relations of rarefied gas dynamics. *Communications in Computational Physics* 2019; 26(3):880-912.
55. Jiang Z, Zhao W, Yuan Z, et al. Computation of hypersonic flows over flying configurations using a nonlinear constitutive model. *AIAA J*; 2019; 57(12): 1-17.
56. Yuan Z, Zhao W, Jiang Z, et al. The application and verification of modified nonlinear coupled constitutive relations model. *AIAA scitech 2019 forum*. Reston: AIAA; 2019.
57. Jiang Z, Chen W, Zhao W. Numerical analysis of the micro-couette flow using a non-newton-fourier model with enhanced wall boundary conditions. *Microfluidics and Nanofluidics* 2017; 22(1):10.
58. Jiang Z, Zhao W, Chen W, et al. Computation of shock wave structure using a simpler set of generalized hydrodynamic equations based on nonlinear coupled constitutive relations. *Shock Waves* 2019; 29(8): 1-13.
59. Liu S, Yang Y, Zhong C. An extended gas-kinetic scheme for shock structure calculations. *Journal of Computational Physics* 2019; 390:1-24.
60. Ayoub RG. Paolo ruffini's contributions to the quintic. *Archive for History of Exact Sciences* 1980; 23(3):253-77.
61. Ohwada T. Structure of normal shock waves: Direct numerical analysis of the boltzmann equation for hard-sphere molecules. *Physics of Fluids A: Fluid Dynamics* 1993; 5(1):217-34.
62. Bird GA, Brady J. *Molecular gas dynamics and the direct simulation of gas flows*. Oxford: Clarendon Press; 1994.

63. Alsmeyer H. Density profiles in argon and nitrogen shock waves measured by the absorption of an electron beam. *Journal of Fluid Mechanics* 1976; 74(3):497-513.
64. Steinhilper EA. Electron beam measurements of the shock wave structure. Part i. The inference of intermolecular potentials from shock structure experiments. Part ii. The influence of accommodation on reflecting shock waves[dissertation]. California: California Institute of Technology;1972.
65. Boyd ID, Chen G, Candler GV. Predicting failure of the continuum fluid equations in transitional hypersonic flows. *Physics of Fluids* 1995; 7(1):210-9.
66. Lofthouse AJ. Nonequilibrium hypersonic aerothermodynamics using the direct simulation monte carlo and navier-stokes models[dissertation]. Michigan: University of Michigan, 2008.
67. Bao FB, Lin JZ, Shi X. Burnett simulation of flow and heat transfer in micro couette flow using second-order slip conditions. *Heat and Mass Transfer* 2006; 43(6):559-66.
68. Gu XJ, Emerson DR. A computational strategy for the regularized 13 moment equations with enhanced wall-boundary conditions. *Journal of Computational Physics* 2007; 225(1):263-83.
69. Plimpton SJ, Moore SG, Borner A, et al. Direct simulation monte carlo on petaflop supercomputers and beyond. *Physics of Fluids* 2019; 31(8):086101.

Appendix A: Roots formula for general quartic equation

The four roots x_0, x_1, x_2 and x_3 for the general quartic equation

$$ax^4 + bx^3 + cx^2 + dx + e = 0 \quad (A1)$$

with $a \neq 0$ are given in the following formula:

$$\begin{cases} x_{0,1} = -\frac{b}{4a} - S \pm \frac{1}{2} \sqrt{-4S^2 - 2p + \frac{q}{S}} \\ x_{2,3} = -\frac{b}{4a} + S \pm \frac{1}{2} \sqrt{-4S^2 - 2p - \frac{q}{S}} \end{cases} \quad (A2)$$

where

$$\begin{cases} p = \frac{8ac - 3b^2}{8a^2} \\ q = \frac{b^3 - 4abc + 8a^2d}{8a^3} \\ S = \frac{1}{2} \sqrt{-\frac{2}{3}p + \frac{1}{3a} \left(Q + \frac{A_0}{Q} \right)} \\ Q = \sqrt[3]{\frac{A_1 + \sqrt{A_1^2 - 4A_0^3}}{2}} \end{cases} \quad (A3)$$

and

$$\begin{cases} A_0 = c^2 - 3bd + 12ae \\ A_1 = 2c^3 - 9bcd + 27b^2e + 27ad^2 - 72ace \end{cases} \quad (A4)$$

Appendix B: Roots formula for general cubic equation

The three roots x_0, x_1 and x_2 for the general cubic equation are given in the following formula:

$$x_k = -\frac{1}{3a} \left(b + \omega^k C + \frac{A_0}{\omega^k C} \right) \quad k = 0, 1, 2 \quad (B1)$$

where

$$\begin{cases} A_0 = b^2 - 3ac \\ A_1 = 2b^3 - 9abc + 27a^2d \\ C = \sqrt[3]{\frac{A_1 \pm \sqrt{A_1^2 - 4A_0^3}}{2}} \\ \omega = \frac{-1 + \sqrt{-3}}{2} \end{cases} \quad (B2)$$